Published in final edited form as:
Br J Ophthalmol. 2012 December ; 96(12): 1522–1529. doi:10.1136/bjophthalmol-2012-301904.

Inflammatory Response to Intravitreal Injection of Gold Nanorods

Michelle Gabriele Sandrian[1,2,3], **Gadi Wollstein**[1,†], **Joel S Schuman**[1,2,3], **Richard A. Bilonick**[1], **Yun Ling**[1], **Hiroshi Ishikawa**[1,2], **Larry Kagemann**[1,2], and **Kyle C. McKenna**[1,4,†]

[1]UPMC Eye Center, Eye and Ear Institute, Ophthalmology and Visual Science Research Center, Department of Ophthalmology, University of Pittsburgh School of Medicine, Pittsburgh, PA

[2]Department of Bioengineering, Swanson School of Engineering, University of Pittsburgh, Pittsburgh, PA

[3]Center for the Neural Basis of Cognition, Carnegie Mellon University and University of Pittsburgh, Pittsburgh, PA

[4]Department of Immunology, University of Pittsburgh, Pittsburgh, PA

Abstract

Aim—To evaluate the utility of gold nanorods (AuNRs) as a contrast agent for ocular optical coherence tomography (OCT).

Methods—Mice were intravitreally injected with sterile AuNRs coated with either poly(strenesulfate) (PSS-AuNRs) or anti-CD90.2 antibodies (Ab-AuNRs), and imaged using OCT. After 24 hours, eyes were processed for transmission electron microscopy or rendered into single cell suspensions for flow cytometric analysis to determine absolute numbers of CD45+ leukocytes and subsets (T cells, myeloid cells, macrophages, neutrophils). Generalized estimation equations were used to compare cell counts between groups.

Results—PSS-AuNRs and Ab-AuNRs were visualized in the vitreous 30min and 24h post-injection with OCT. At 24h, a statistically significant increase in leukocytes, comprised primarily of neutrophils, was observed in eyes that received either AuNR in comparison to eyes that received saline. The accumulation of leukocytes was equal in eyes given PSS-AuNR or Ab-AuNR. Endotoxin-resistant C3H/HeJ mice also showed ocular inflammation after injection with AuNRs, indicating that the inflammatory response was not due to lipopolysaccharide contamination of AuNRs.

Conclusions—Although AuNRs can be visualized in the eye using OCT they can induce ocular inflammation, which limits their use as a contrast agent.

Keywords

gold nanoparticles; optical coherence tomography; contrast enhancement; immune response

[†]Please address correspondence to either: Gadi Wollstein, UPMC Eye Center, 203 Lothrop Street, Eye and Ear Institute, Room 834.1, Pittsburgh, PA 15213; wollsteing@upmc.edu, or Kyle C. McKenna, UPMC Eye Center, 203 Lothrop Street, Eye and Ear Institute, Room 910, Pittsburgh, PA 15213; mckennakc@upmc.edu.

Author Contributions: design of the study (MGS, GW, KCM), conduction of the study (MGS, GW, KCM), data analysis and interpretation (MGS, GW, RAB, YL, KCM, HI), manuscript preparation (MGS), manuscript review (GW, JSS, HI, LK, KCM), manuscript final approval (MGS, GW, KCM).

Competing Interests: Dr. Schuman received royalties for intellectual property licensed by Massachusetts Institute of Technology to Carl Zeiss Meditec.

Nanoparticles are receiving increased attention in ophthalmology as molecular contrast agents for optical imaging.[1] Metallic nanoparticles, such as gold nanorods (AuNRs), may be particularly useful for optical imaging given their localized surface plasmon resonant (SPR) response, a collective oscillation of conduction-band electrons that facilitates strong scattering and absorption of light.[2] It is possible to tune the SPR wavelength of AuNRs by adjusting their aspect ratio, making them attractive for imaging with ophthalmic optical coherence tomography (OCT), where light sources with a center wavelength of around 850nm are often used for retinal imaging.[3] In addition, AuNRs can be functionalized with antibodies,[4–6] which may be applied to target specific structures of interest to provide contrast.

Investigation into the use of gold nanoparticles as exogenous contrast agents for OCT has been growing. Several groups have demonstrated the potential for gold nanoshells,[7–9] nanocages,[10] and AuNRs[11,12] as contrast agents in OCT imaging. Despite many studies indicating the potential for gold nanoparticles in OCT imaging in general, the literature is surprisingly devoid of information regarding *in vivo* ophthalmic applications of gold nanoparticles.

Studies have shown that certain nanoparticles can be toxic depending on size, shape or surface chemical characteristics,[13–16] and there is evidence that gold nanoparticles elicit an undesired immune response.[17,18] Therefore, before AuNRs can be considered for contrast enhancement *in vivo*, their effect on the eye must also be taken into consideration. The aim of this study was to evaluate the utility of AuNRs as a contrast agent in the eye by first determining if AuNRs could be visualized in the eye by OCT, and then by carefully evaluating whether AuNRs induced ocular inflammation.

Materials and Methods

Mice

C57Bl/6 mice, C3HeB/FeJ and C3H/HeJ mice (Jackson Laboratory, Bar Harbor, ME) were used. All mice were maintained in the University of Pittsburgh Animal Facility with a 12-hour light/dark cycle and free access to water and standard laboratory feed. All experimentation was approved by the University of Pittsburgh's Institutional Animal Care and Use Committee and adhered to the ARVO Statement for the Use of Animals in Ophthalmic and Vision Research.

Gold Nanorods

AuNRs resonant at a wavelength of ~850nm were synthesized by Nanorods (Germantown, MD), using a wet chemical synthesis approach with a surfactant as a scaffold for growing rods from spherical colloidal gold seed particles.[19] A colloidal gold spherical seed solution is added to a surfactant-based growth solution, and growth of the colloidal particles occurs along a single axis, forming the longitudinal dimension of the rod. AuNRs were coated with antibodies (α-CD90.2) and a polymer (poly(strenesulfate); PSS), or just PSS alone. Negatively charged PSS is a detergent used to detoxify the AuNRs by displacing and neutralizing positively charged cetyl trimethylammonium bromide (CTAB) surfactant. Anti-CD90 (Thy1) antibodies were chosen to create antibody coated (Ab-AuNRs) since Thy1 is expressed on the surface of retinal ganglion cells.[20] Both the Ab-AuNR and PSS-AuNR solutions had an optical density (OD) ~50. AuNR solutions (1μl), were cultured on chocolate agar medium (BD Diagnostic Systems, Sparks, MD) and incubated at 36°C under 6% CO_2 at atmospheric conditions for 3 days to evaluate bacterial contamination. Only solutions free of bacterial contamination were used.

Ocular Injections

Animals were anesthetized with an intraperitoneal injection of ketamine (Ketaject, Phoenix Pharmaceuticals, St. Joseph, MI; 80 mg/kg) and xylazine (Xyla-ject, Phoenix Pharmaceuticals; 5 mg/kg) prior to the injection. The eye was proptosed using forceps and an incision was made at the limbus by the insertion of a 30-gauge needle. A 33-gauge hypodermic needle fitted on a Hamilton 700 series microsyringe (Hamilton, Reno, NV) was then inserted into the incision site to administer a 2μl intravitreal injection. The procedure was performed under a surgical microscope in both eyes per animal. Unconjugated PSS-AuNRs (λ_{spr} = 850nm) and Ab-AuNRs (λ_{spr} = 857nm) with an aspect ratio of ~3.4 were used for nanoparticle injections. Phosphate-buffered saline (PBS) was used for sham injections.

OCT Imaging

Prior to imaging, animals were anesthetized as described above. Tropicamide (1%; Falcon Pharmaceuticals, Fort Worth, TX) was applied topically for pupil dilation. A thin glass cover slip was coupled to the cornea using Hydroxymethylcellulose ophthalmic demulcent solution (Goniosol 2.5%; Akon, Buffalo Grove, IL). Mice were secured on a custom stage, which allowed for free rotation. Spectral-domain (SD-)OCT scans of the retina, vitreous and posterior lens were acquired using a SD-OCT system (Bioptigen, Durham, NC), modified with a broadband super luminescent diode (Superlum, Dublin, Ireland; λ = 870nm, $\Delta\lambda$ = 200nm). The scanning area consisted of a 1.5×1.5×2mm region (250×250×1024 pixels) at the surface of coverslip; with four consecutively repeated axial scans averaged at each sampling location. Baseline images were acquired before injection.

Collagenase digestion of eyes for flow cytometry

24 hours post-injection, mice were euthanized and both eyes enucleated. Eyes were immediately washed in PBS to remove any excess blood then transferred into a 2ml solution consisting of 1mg/ml collagenase IV (Sigma, St. Louis, MO) 0.25mg/ml deoxyribonuclease I (Sigma) and 1% fetal bovine serum (FBS; Atlanta Biologicals, Lawrenceville, GA) in RPMI 1640 media (Mediatech, Manassas, VA). Eyes were gently chopped with scissors to increase surface area for digestion, and then incubated at 37°C for 1.5 hours. The solution was resuspended after 45 minutes to accelerate the formation of a single cell suspension.

After digestion, eye solutions were filtered through a nylon screen (70μm), washed with PBS and resuspended in 400μl FACS buffer (PBS + 1%FBS). One-quarter of each eye solution (100μl) was added to a 96 well plate and samples were incubated with unconjugated anti-CD16/CD32 antibodies (BD Pharmingen, San Diego, CA) for 10 minutes on ice in the dark to block Fc receptors. Wells were washed with FACS buffer and stained with a mix of fluorescently labeled antibodies (BD Biosciences, San Jose, CA) for 20 minutes on ice in the dark. This mix consisted of PerCP conjugated αCD45, PE conjugated αThy1.2, Pacific blue conjugated αCD11b, FITC conjugated αGR-1, and Allophycocyanin conjugated αF4/80 to allow for characterization of infiltrating $CD45^+$ leukocytes as $Thy1.2^+$ T cells, $CD11b^+$ myeloid cells, $CD11b^+$ $F4/80^+$ $GR\text{-}1^-$ macrophages, and $CD11b^+$ $F4/80^-$, $GR\text{-}1^+$ neutrophils. Isotype controls for each antibody were used to set gates to distinguish leukocyte subsets. CountBright Absolute Counting Beads (Invitrogen, Camarillo, CA) were added to ocular cell suspensions to determine the absolute number of cells of respective immune cell populations through analysis performed using FlowJo software (Tree Star, Ashland, OR). The absolute number of cells (N_{abs}) was determined as follows:

$$N_{abs}=4\,\frac{b_a}{b_c}\,N,$$

where b_a and b_c are the number of beads added and the number of beads collected, respectively, and N is the number of cells counted for a specific population (all leukocytes, T cells, myeloid cells, macrophages or neutrophils).

Transmission electron microscopy (TEM) Two mice were sacrificed 24 hours post-injection of Ab-AuNR. Eyes were enucleated and immersion fixed in 2.5% glutaraldehyde overnight at 4°C. The retina, posterior lens and vitreous washed and post-fixed in aqueous 1% OsO_4, 1% $K_3Fe(CN)_6$. The tissue was dehydrated and infiltrated in 1:1 mixture of propylene oxide:Polybed 812 epoxy resin (Polysciences, Warrington, PA). This was embedded in molds and ultrathin (60nm) sections of the vitreous were collected on copper grids and stained. Sections were imaged using a JEOL JEM 1210 TEM (Peabody, MA) at 80kV fitted with a side-mount AMT 2k digital camera (Advanced Microscopy Techniques, Danvers, MA).

Statistical Analysis

Generalized estimation equations were fitted to model cell counts, taking into account clustering between eyes from the same animal. An α-level of 0.05 was the cutoff for statistical significance.

Results

Visualization of AuNRs

Fourteen C57Bl/6 (25 eyes; age 127 days) mice were used, with two eyes from two different mice processed for TEM and the remaining eyes for flow cytometry. To determine if AuNRs could be visualized in the eye by OCT, mice were injected with AuNRs in the vitreous, and OCT images were taken in live animals approximately 30 minutes and 24 hours post-injection. As shown in representative images in Figure 1, there is an increase in backscatter observed in the vitreous of AuNR injected mice that was not present in the baseline image, or in mice receiving a sham PBS injection (Figure 2). These data indicate that AuNRs can be visualized within the eye by OCT. Twenty-four hours after injection, a strong signal was still observed in the vitreous of eyes injected with AuNRs (Figures 1 and 2), while the vitreous of eyes given sterile PBS remained essentially transparent.

TEM was used to confirm the presence of AuNRs in the eye. Figure 3 shows that, at 24 hours, AuNRs were primarily clustered extracellularly in strands of the vitreous and were not observed within the retina. AuNRs were in close proximity to, surrounded by, or engulfed by mononuclear cells, suggesting that an inflammatory response had ensued.

Ocular Inflammation after AuNR injection

To carefully characterize ocular inflammation in AuNR injected mice, flow cytometric analysis of single cell suspensions of collagenase-digested eyes was used. Four groups of C57Bl/6 mice were evaluated: untreated (Group 1; 6 eyes), sterile PBS injection (Group 2; 6 eyes), unconjugated AuNR injection (Group 3; 5 eyes) and Ab-AuNR injection (Group 4; 6 eyes). Anti-CD45 antibodies were used to distinguish between immune and ocular cells since CD45 is expressed exclusively by bone-marrow derived cells.

Injection of either antibody-conjugated or unconjugated AuNRs resulted in a similar and statistically significant increase in CD45+ cells within the eye, indicating ocular inflammation (Figure 4). In contrast, CD45+ cell numbers in mice injected with sterile PBS were similar to untreated mice, indicating that inflammation was not due to trauma induced by the injection.

To further characterize the immune infiltrate, CD45+ cells were stained with antibodies to Thy 1.2 to identify T cells and CD11b to identify myeloid cells. Anti-F4/80 and anti-GR-1 antibodies were used to further distinguish CD11b+ cells as macrophages or neutrophils, respectively. CD45+ cells infiltrating eyes of AuNR-injected mice were predominantly CD11b+GR-1+ neutrophils, followed by CD11b+ F4/80+ macrophages (Figure 4). A moderate, albeit significant increase in T cells was observed in mice given antibody conjugated AuNRs.

Excluding Endotoxin Contamination as a Cause of Inflammation

The previous experiments suggested that AuNRs were inflammatory. Although AuNRs were tested to rule out bacterial contamination prior to use, it was still possible that endotoxin (lipopolysaccharide, LPS) – which is not detectable using standard bacterial culture techniques – was an inflammatory mediator. To evaluate the potential contribution of endotoxin contamination in our system we used C3H/HeJ mice, which are resistant to endotoxin due to a defect in toll-like receptor 4.[21] C3H/HeJ mice (age 63 days) received an intravitreal injection of sterile PBS (Group 7; 4 eyes) or were injected with unconjugated AuNRs (Group 8; 4 eyes), and were compared to similarly treated groups of endotoxin-sensitive C3HeB/FeJ mice (age 63 days), Groups 5 (6 eyes) and 6 (4 eyes), respectively.

Both C3HeB/FeJ endotoxin-sensitive and C3H/HeJ endotoxin-resistant mice that received a PSS-AuNR injection showed a consistent trend of increased inflammatory cell numbers compared to those receiving a PBS injection, although there was a difference in absolute number of inflammatory cells across strains and cell types (Figure 5). Statistically significant increases in CD45+ cells, including CD11b+ myeloid cells, were observed. There was not a statistically significant increase in the number of F4/80+ macrophages for either strain, but there were significant increases in the number of GR-1+ neutrophils that was consistent with our previous experiments (Figure 4). In addition, there was not a statistically significant increase in the Thy 1 T cell count for endotoxin-sensitive mice, but there was for endotoxin-resistant C3H/HeJ mice. These data indicated that ocular inflammation after nanoparticle injection was not due to endotoxin contamination of nanoparticles.

Discussion

We were able to visualize AuNRs in the vitreous using OCT immediately after intravitreal injection. AuNRs increased the backscattered signal in the vitreous but obscured the retinal signal and induced ocular inflammation that was not attributed to bacterial or endotoxin contamination.

It is possible the reagents used during the production of AuNRs could be inflammatory. For example, trace amounts of CTAB surfactant may lead to inflammation. CTAB is a necessary scaffold for longitudinal growth of the AuNRs during synthesis, and excess surfactant is removed via centrifugation once AuNRs have formed. Some remaining CTAB is unavoidable, however, since eliminating it all would cause nanoparticle aggregation. The addition of a negatively charged polymer coating neutralizes CTAB to prevent protein aggregation and provides a shield of protection against CTAB exposure. However, it is also possible that PSS, the polymer coating used here to modify the AuNR surface, is not completely shielding all CTAB, or that CTAB is released with time. Although PSS is considered safe for *in vivo* applications,[22] we cannot exclude the possibility that it is inflammatory within the eye. An alternate polymer, such as polyethylene glycol, may reduce the extent of inflammation and provide better shielding. Future studies optimizing coatings are warranted.

A recent study evaluated the ability of polymeric nanoparticles to reach and penetrate the internal limiting membrane to enter the retina for drug delivery applications.[23] Although they did not evaluate inflammation associated with these nanoparticles, the authors demonstrated the importance of surface charge on the diffusion of nanoparticles, showing that anionic particles can enter the retina while cationic particles stick to the lens and the vitreous. Interestingly, the anionic particles were substantially larger (210–340nm diameter) than the AuNRs used in this study, but were still able to diffuse through internal limiting membrane. Thus, it might be preferable to create anionic conditions for retinal delivery of contrast agents.

The aspect ratio of the AuNRs in this study was chosen to align the SPR wavelength with current commercial ophthalmic OCT devices. However, shape also appears to affect the extent to which nanoparticles are phagocytosed by inflammatory cells,[24] which, therefore, may affect movement through the vitreous. Different sizes of nanoparticles with a consistent aspect ratio must also be evaluated to see if nanoparticle diffusion through the vitreous can be improved.

The high magnification TEM images (Figure 3) show a vast network of fibers in the vitreous, which appear to be trapping AuNRs. Recently, a method for phagocytosis-independent extracellular removal of bacteria, neutrophil extracellular traps (nanoNETs), was discovered and shown to occur in the clearance of nanoparticles.[25] Granulocytes, monocytes and macrophages can form nanoNETs, which are comprised of DNA and protein. Our observations that neutrophils were the primary infiltrate of AuNR injected eyes and that AuNRs were primarily surrounded by vitreal strands is highly suggestive of neutrophil-mediated nanoNETs. Additional studies are necessary to determine whether the structures observed in our TEM images match those of the nanoNETs and are responsible for trapping AuNRs and preventing movement through the vitreous.

In summary, our findings suggest that AuNRs can be visualized in the vitreous but elicit an inflammatory response. This response may present an obstacle for using AuNRs as contrast agents with OCT imaging in the eye. Further studies are planned to determine whether AuNR design modifications can minimize inflammation. Once inflammation has been minimized, studies evaluating clearance and determining the long-term effects of AuNRs on the eye are the logical next steps. The flow cytometric approach we present offers the advantage of objective quantification of the inflammatory infiltrate in the whole eye, and thus should be a valuable tool for optimizing the biocompatibility of all types of nanoparticles after they are introduced into the eye.

Acknowledgments

Support: NIH R21-EY019092, R01-EY013178, P30-EY008098; Eye and Ear Foundation (Pittsburgh, PA); Research to Prevent Blindness

The authors would like to thank Regis Kowalski (Department of Ophthalmology, University of Pittsburgh School of Medicine) for assistance assessing the sterility of the gold nanorods used in these experiments, and Ming Sung, Jonathan Franks, Donna Stolz, PhD and Simon Watkins, PhD (Center for Biologic Imaging, University of Pittsburgh) for transmission electron microscopy sample preparation.

References

1. Diebold Y, Calonge M. Applications of nanoparticles in ophthalmology. Prog Retin Eye Res. 2010:596–609. [PubMed: 20826225]
2. Oldenburg SJ, Averitt RD, Westcott SL, et al. Nanoengineering of optical resonances. Chem Phys Lett. 1998; 288:243–7.

3. Boppart SA, Oldenburg AL, Xu C, et al. Optical probes and techniques for molecular contrast enhancement in coherence imaging. J Biomed Opt. 2005; 10:41208. [PubMed: 16178632]
4. El-Sayed IH, Huang X, El-Sayed MA. Surface plasmon resonance scattering and absorption of anti-EGFR antibody conjugated gold nanoparticles in cancer diagnostics: applications in oral cancer. Nano Lett. 2005; 5:829–34. [PubMed: 15884879]
5. Sokolov K, Follen M, Aaron J, et al. Real-time vital optical imaging of precancer using anti-epidermal growth factor receptor antibodies conjugated to gold nanoparticles. Cancer Res. 2003; 63:1999–2004. [PubMed: 12727808]
6. Huang X, El-Sayed IH, El-Sayed MA. Applications of gold nanorods for cancer imaging and photothermal therapy. Methods Mol Biol. 2010; 624:343–57. [PubMed: 20217607]
7. Loo C, Lin A, Hirsch L, et al. Nanoshell-enabled photonics-based imaging and therapy of cancer. Technol Cancer Res Treat. 2004; 3:33–40. [PubMed: 14750891]
8. Lin AW, Lewinski NA, West JL, et al. Optically tunable nanoparticle contrast agents for early cancer detection: model-based analysis of gold nanoshells. J Biomed Opt. 2005; 10:064035. [PubMed: 16409100]
9. Agrawal A, Huang S, Wei Haw Lin A, et al. Quantitative evaluation of optical coherence tomography signal enhancement with gold nanoshells. J Biomed Opt. 2006; 11:041121. [PubMed: 16965149]
10. Cang H, Sun T, Li ZY, et al. Gold nanocages as contrast agents for spectroscopic optical coherence tomography. Opt Lett. 2005; 30:3048–50. [PubMed: 16315717]
11. Troutman TS, Barton JK, Romanowski M. Optical coherence tomography with plasmon resonant nanorods of gold. Opt Lett. 2007; 32:1438–40. [PubMed: 17546147]
12. Oldenburg AL, Hansen MN, Zweifel DA, et al. Plasmon-resonant gold nanorods as low backscattering albedo contrast agents for optical coherence tomography. Opt Express. 2006; 14:6724–38. [PubMed: 19516854]
13. Pernodet N, Fang X, Sun Y, et al. Adverse effects of citrate/gold nanoparticles on human dermal fibroblasts. Small. 2006; 2:766–73. [PubMed: 17193121]
14. Goodman CM, McCusker CD, Yilmaz T, et al. Toxicity of gold nanoparticles functionalized with cationic and anionic side chains. Bioconjug Chem. 2004; 15:897–900. [PubMed: 15264879]
15. Chithrani BD, Chan WC. Elucidating the mechanism of cellular uptake and removal of protein-coated gold nanoparticles of different sizes and shapes. Nano Lett. 2007; 7:1542–50. [PubMed: 17465586]
16. Pan Y, Neuss S, Leifert A, et al. Size-dependent cytotoxicity of gold nanoparticles. Small. 2007; 3:1941–9. [PubMed: 17963284]
17. Dobrovolskaia MA, McNeil SE. Immunological properties of engineered nanomaterials. Nat Nanotechnol. 2007; 2:469–78. [PubMed: 18654343]
18. Cho WS, Cho M, Jeong J, et al. Acute toxicity and pharmacokinetics of 13 nm-sized PEG-coated gold nanoparticles. Toxicol Appl Pharmacol. 2009; 236:16–24. [PubMed: 19162059]
19. Nikoobakht B, El-Sayed MA. Preparation and growth mechanism of gold nanorods (NRs) using seed-mediated growth method. Chem Mater. 2003; 15:1957–62.
20. Zhang J, Wu SM, Gross RL. Effects of beta-adrenergic blockers on glutamate-induced calcium signals in adult mouse retinal ganglion cells. Brain Res. 2003; 959:111–9. [PubMed: 12480164]
21. Poltorak A, He X, Smirnova I, et al. Defective LPS signaling in C3H/HeJ and C57BL/10ScCr mice: mutations in Tlr4 gene. Science. 1998; 282:2085–2088. [PubMed: 9851930]
22. Shepherd G, Klein-Schwartz W, Burstein AH. Efficacy of the cation exchange resin, sodium polystyrene sulfonate, to decrease iron absorption. J Toxicol Clin Toxicol. 2000; 38:389–94. [PubMed: 10930055]
23. Koo H, Moon H, Han H, et al. The movement of self-assembled amphiphilic polymeric nanoparticles in the vitreous and retina after intravitreal injection. Biomaterials. 2012; 33:3485–3493. [PubMed: 22322197]
24. Champion JA, Mitragotri S. Shape induced inhibition of phagocytosis of polymer particles. Pharm Res. 2009; 26:244–9. [PubMed: 18548338]

25. Bartneck M, Keul HA, Zwadlo-Klarwasser G, et al. Phagocytosis independent extracellular nanoparticle clearance by human immune cells. Nano Lett. 2010; 10:59–63. [PubMed: 19994869]

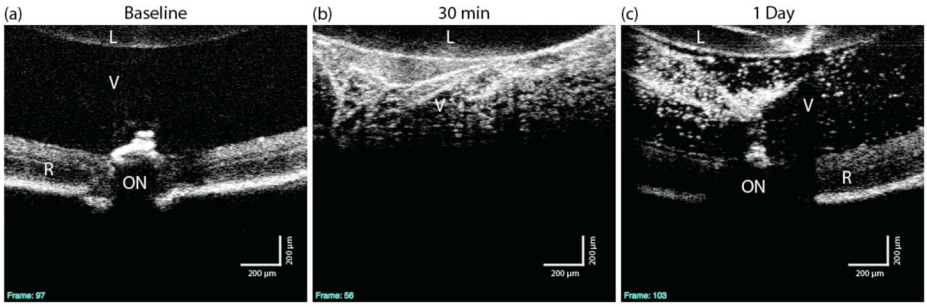

Figure 1.

OCT images from a single mouse, before and after PSS-AuNR injection. Single cross-sections (a–c). The retina is completely obscured by the presence of the scattering PSS-AuNRs 30 min post injection.

L: Lens, V: Vitreous, R: Retina, ON: Optic Nerve

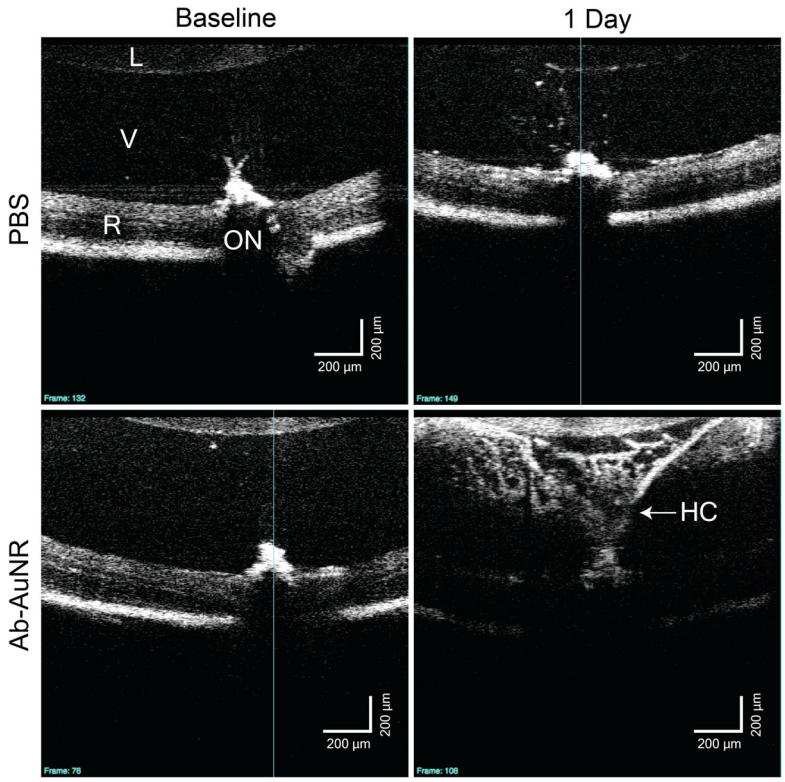

Figure 2.

Baseline and 1 day after injection images from mice injected with sham (PBS) and antibody conjugated gold nanorods (Ab-AuNR). Marked signal enhancement is observed in the Ab-AuNR injected vitreous as compared to both pre-injection and the sham injection images. The retinal signal is attenuated in the Ab-AuNR injected eye due to a shadowing effect caused by the strong backscattering signal from the vitreous.

L: Lens, V: Vitreous, R: Retina, ON: Optic Nerve, HC: Hyaloid Canal

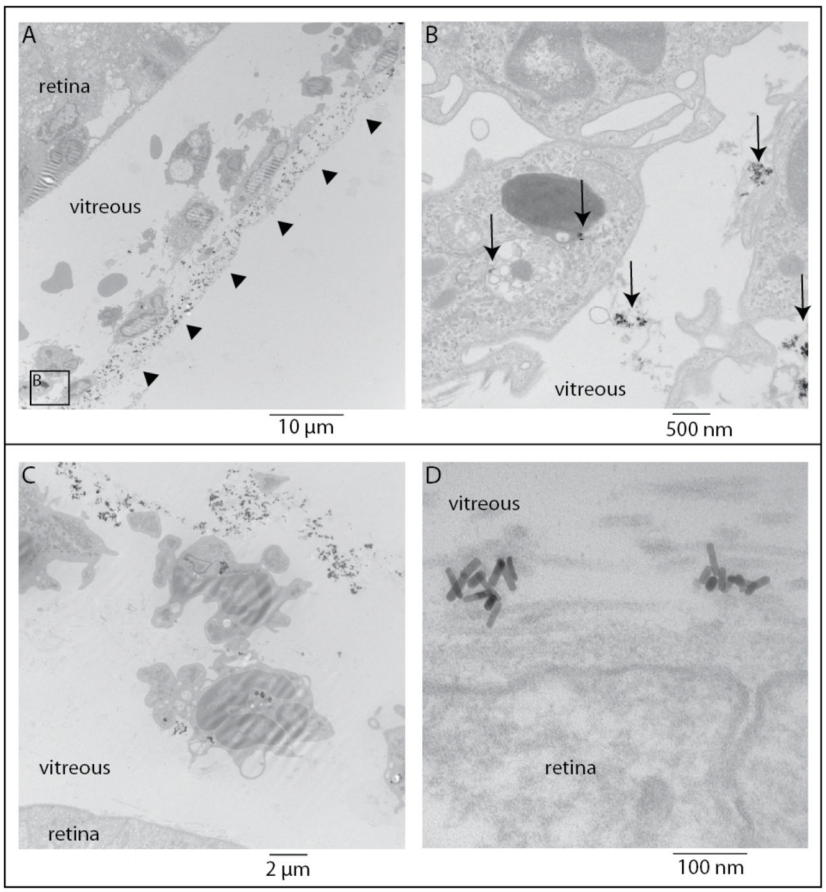

Figure 3.
Transmission electron microscopy images from two C57Bl/6 mice (top and bottom panels) 24 hours post antibody conjugated gold nanorods (Ab-AuNR) injection. (A) Arrowheads show a line of extracellular particles near inflammatory cells and (B) arrows show extracellular particles as well as some that have been phagocytosed. (C) intra- and extracellular Ab-AuNRs are evident in the vitreous and near the internal limiting membrane of the retina (D).

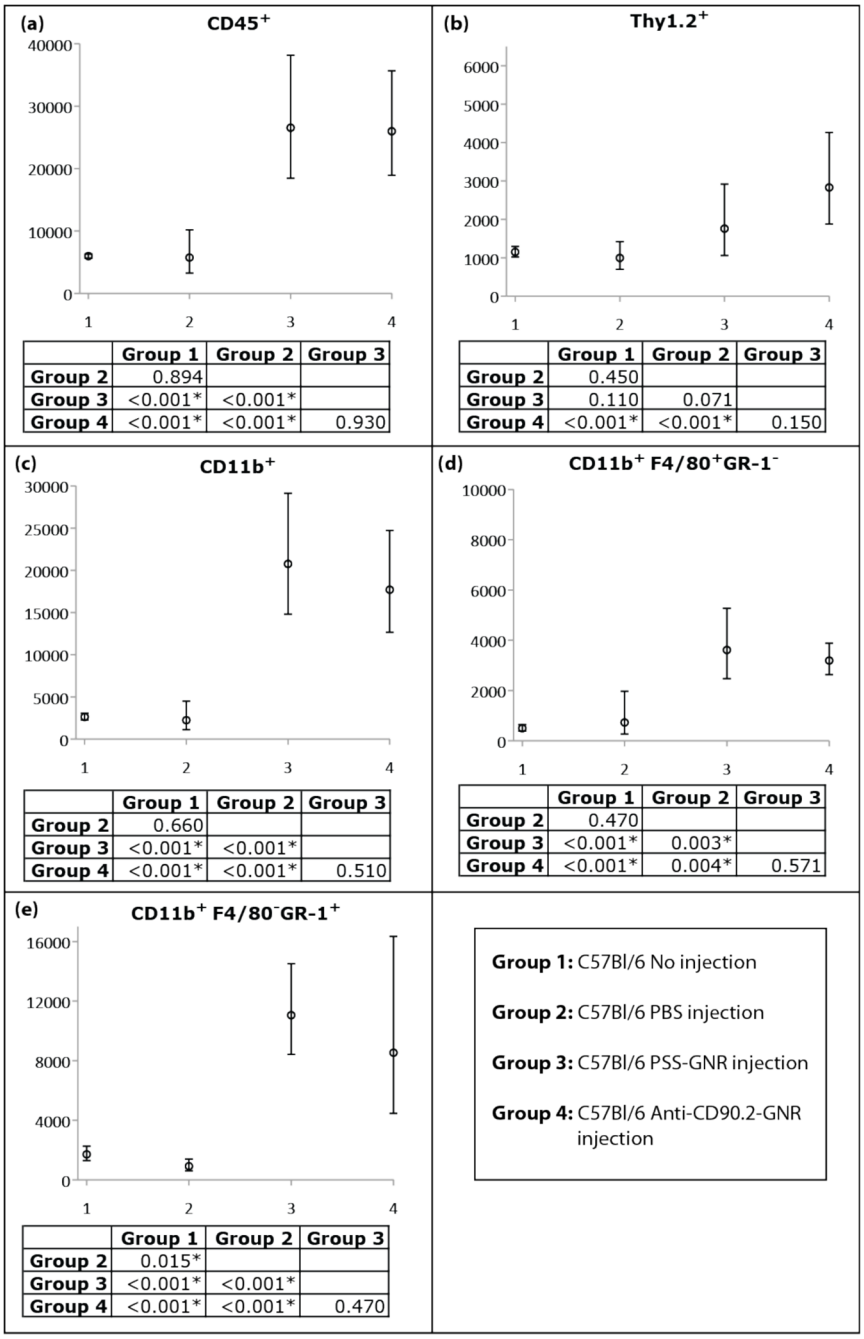

Figure 4.

Expected cell counts and 95% confidence intervals from generalized estimation equation models of cell counts for C57Bl/6 (a) CD45+ leukocytes that expressed (b) Thy1.2, or (c) CD11b, and CD11b+ cells that expressed (d) F4/80 and (e) GR-1. P-values for pairwise comparison of groups for a given cell type are presented, with statistically significant differences indicated by *.

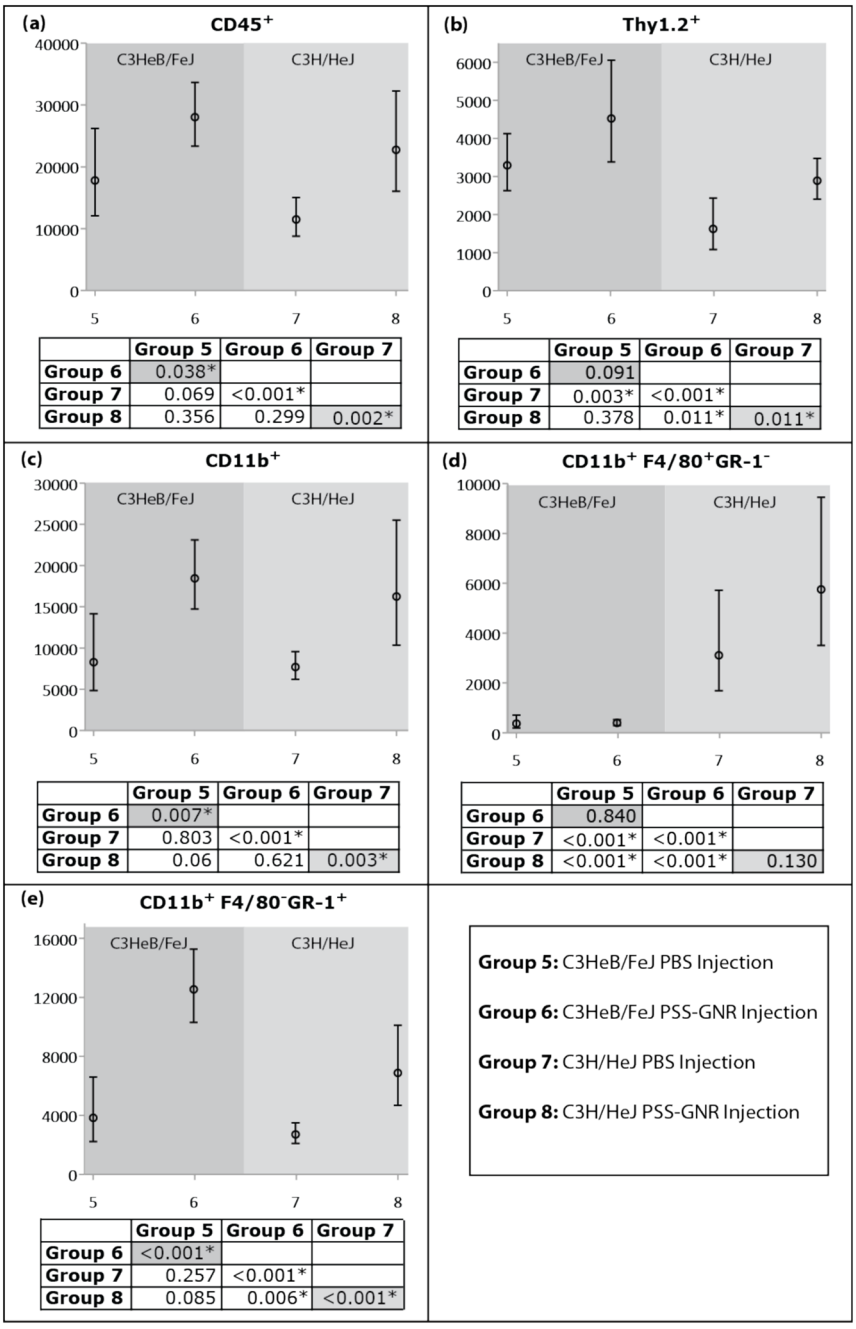

Figure 5.

Expected cell counts and 95% confidence intervals from generalized estimation equation models of cell counts for C3HeB/FeJ and C3H/HeJ (a) CD45+ leukocytes that expressed (b) Thy1.2, or (c) CD11b, and CD11b+ cells that expressed (d) F4/80 and (e) GR-1. P-values for pairwise comparison of groups for a given cell type are presented, with statistically significant differences indicated by *.